Miniature Coil Array for Passive Magnetocardiography in Non-Shielded Environments

Keren Zhu, *Student Member, IEEE*, Adhvait M. Shah, Jan Berkow, and Asimina Kiourti, *Senior Member, IEEE*

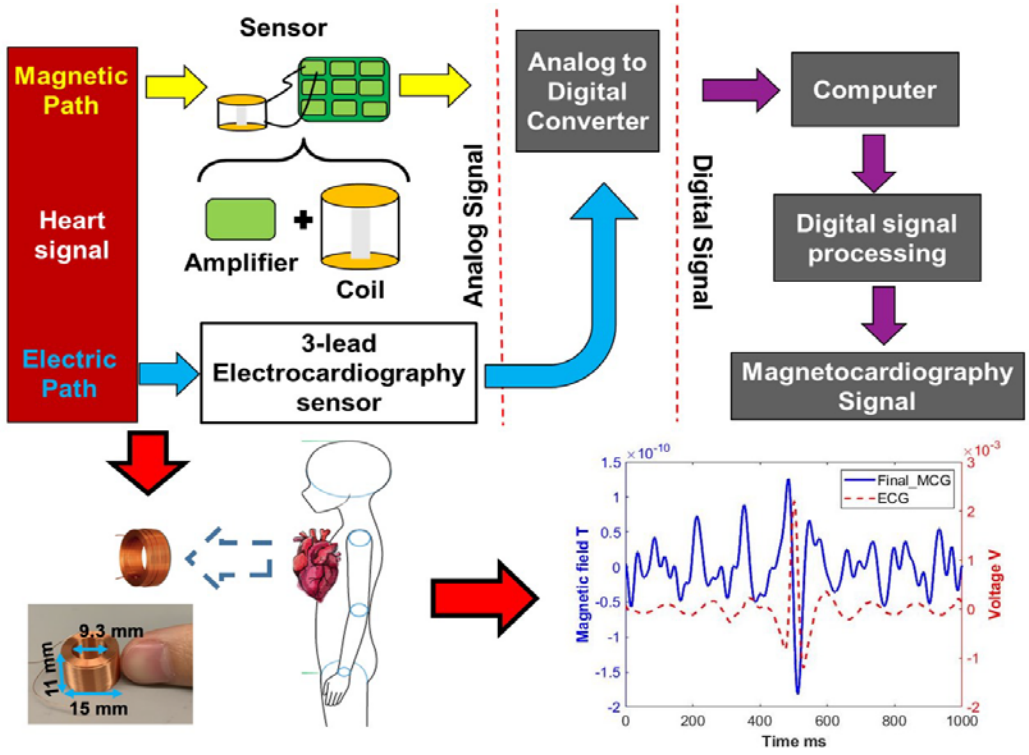

Operating principle of a miniature coil array for passive magnetocardiography sensing in non-shielded environments.

Take-Home Messages

- We report miniaturized coil sensors combined with advanced digital signal processing (DSP) to passively detect the magnetic fields radiated by the human body without the need for shielding.
- *In vitro* experiments confirm that emulated human magnetocardiography (MCG) signals can readily be detected in non-shielded environments using our proposed coil array.
- Monitoring the magnetic fields that are naturally emanated by the human body (such as the heart) can help diagnose several health conditions, including myocardial ischemia, arrhythmia, right atrial hypertrophy, right ventricular hypertrophy, and the Brugada syndrome.
- Our coil sensor overcomes limitations in state-of-the-art MCG systems that require extensive shielding and/or bulky and expensive devices.
- Leveraging our proposed 3D-printed coil fixtures, arrays of diverse number of coils and pattern configurations can be employed to fit diverse clinical needs and to further reduce the recording time.

Miniature Coil Array for Passive Magnetocardiography in Non-Shielded Environments

Keren Zhu, *Student Member, IEEE,* Adhvait M. Shah, Jan Berkow, and Asimina Kiourti, *Senior Member, IEEE*

Abstract Existing practices for monitoring heart activity rely heavily on electrocardiography (ECG) approaches, which suffer from low accuracy (as electric fields get impacted by biological tissues); extensive diagnostic times; and lack of comfort (as electrodes are in direct contact with the human body). Though magnetocardiography (MCG) provides more accurate and localized signals while also being non-contact, state-of-the-art equipment for capturing such weak magnetic fields (i.e., SQUIDs) requires extensive shielding and is very expensive. MCG sensing devices that do not require shielding have been reported, but they are bulky, heavy, and cumbersome to use. In this work, we take a major step forward and propose a novel, miniature, and low-cost MCG sensor for operation in non-shielded environments that breaks the state-of-the-art boundaries in terms of size and weight. Our sensor relies on novel coil design principles and Digital Signal Processing (DSP) algorithms to achieve: (a) 4.67 times smaller diameter, (b) 4.5 times smaller height, and (c) at least 216 times lighter weight than previous passive implementations. *In vitro* measurements demonstrate that a 4-coil sensor array with 15 minutes of recording time is sufficient to capture human MCG signals. Discussions indicate that higher number of coils and longer recording times can be employed to improve the signal clarity and fit diverse clinical needs. The proposed coil sensor array provides a convenient method to diagnose several cardiac conditions, such as myocardial ischemia, arrhythmia, right atrial hypertrophy, right ventricular hypertrophy, and the Brugada syndrome.

***Keywords* — Bioelectromagnetics, Faraday's law, induction coils, magnetocardiography.**

I. Introduction

Electromagnetic (EM) fields are generated by different areas across the human body as attributed to current flowing through the underlying organs. As would be expected, abnormal organ function alters the EM fields being generated. In turn, monitoring and analyzing EM fields that are naturally emanated by the human body is critical in the detection and diagnosis of numerous health conditions. For example, EM fields generated by the human heart can help identify several cardiac defects [1], such as myocardial ischemia [2], arrhythmia [3], right atrial hypertrophy [4], right ventricular hypertrophy, and the Brugada syndrome [4].

Existing practices for monitoring heart activity rely heavily on sensing the cardiac electric potential across the chest surface and is known as electrocardiography (ECG) [5]. However, ECG suffers from several limitations. First, the equipment used to capture ECG signals relies on electrode pads that are in direct contact with the human body, making it an uncomfortable procedure [6]. In addition, many people suffer from skin irritation and allergy reaction underneath the skin where the electrode pads are placed [7]. Second, due to the fact that electric signals are attenuated by the lossy human tissues, ECG has very low accuracy in detecting deep tissue signals [8]. Third, ECG can only provide two-dimensional views of the cardiac activity and typically requires extensive time for accurate diagnosis [9].

As an alternative to ECG, magnetocardiography (MCG) can provide much more clinically relevant information in assessing cardiac activity [10]. MCG measures the magnetic fields generated by the heart as captured upon the chest area and has the ability to provide much more accurate and localized cardiac signal images as compared to ECG while also being non-contact [4]. However, the major challenge associated with MCG lies in the weak magnitude of the sensed magnetic fields. These are typically in the order of 10^{-6} Gauss [11], i.e., 10^{-6} times lower than the earth's magnetic field [12]. As a result, MCG signals are typically captured using superconducting quantum interface devices (SQUIDs) that require expensive helium cooling and extensive shielding. In turn, SQUIDs are very expensive to operate [13]. For example, the SQUID set-up used in the Elekta Neuromag TRIUX costs around 1 million USD, and due to the use of cryogenic cooling, the cost of operation is around 5000 USD [14]. High-Tc SQUID-based systems also require cooling (typical operating temperature is 77K [15]), yet are less expensive. In particular, some works changed the cryogen from liquid helium to nitrogen to reduce cost [15], while others employed cryocoolers to simplify the system and ease its handling [16]. Despite the lower cost, high-Tc

This work was supported by the Defense Health Agency under contract no. W81XWH-17-C-0131.

K. Zhu and A. Kiourti are with the ElectroScience Laboratory, Department of Electrical and Computer Engineering, The Ohio State University, Columbus, OH 43221 USA (e-mail: zhu.1266@osu.edu, kiourti.1@osu.edu).

A.M. Shah and J. Berkow are with Triton Systems Inc., Chelmsford, MA 01824 USA (e-mail: amshah@tritonsys.com, jberkow@tritonsys.com).

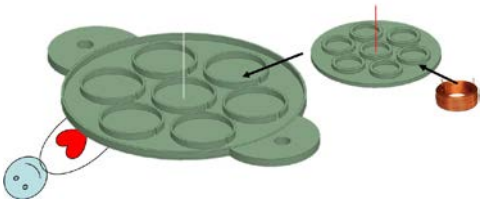

Fig. 1. Overview of coil array placement upon a subject.

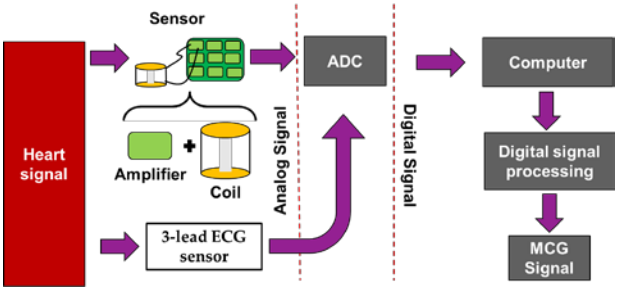

Fig. 2. Overview of the proposed passive coil sensing system.

SQUID-based systems are still bulky as they require large spaces to fit the cooling structure, and often require sophisticated fabrication and high quality thin films to achieve the target noise levels [15]. For other types of magnetometers that do not rely on cooling, bulkiness and complexity remain major challenges against their widespread adoption [17]-[24]. For example, atomic magnetometers require additional space for the laser pump, vacuum packing and heating structure, and can only operate in narrow frequency bandwidths [17]-[20]. The atomic magnetometer in [21] requires the sensor vapor to be heated to over 150°C, while magnetoimpedance (MI) gradiometers must be used in combination with induction coils and high frequency AC currents [22] [23], and in some cases, active shielding [24]. On top of the above, a major challenge for MI gradiometers is the low sensitivity: even with active shielding, the main spike R-wave can barely be identified from the noise floor in [24]. As an alternative, recent works have reported induction coil magnetometers for MCG sensing [25]. The limitation in this case lies in the use of bulky and heavy coil arrays with embedded iron core.

In this work, we take a major step forward and propose a novel, miniature, and low-cost MCG sensor for operation in non-shielded environments that breaks the state-of-the-art boundaries in terms of size and weight. The sensor's operating principle builds on [25], and relies on: (a) novel induction coils that capture the weak magnetic field radiated by the heart, and (b) new signal post-processing algorithms to de-noise the signal. Our approach brings forward a novel MCG sensor that is: (a) 4.67 times smaller in diameter, (b) 4.5 times smaller in height, and (c) at least 216 times lighter than [25] (based on approximate calculations since no exact weight measurements were reported in [25]). Besides the convenience and portability aspects associated with our proposed design, an additional advantage is that a larger number of sensors can now be embedded within a given surface area. This implies MCG imaging of much higher resolution as compared to [25].

Specifically, the MCG sensing coils reported in this work are designed based on the model of a tightly winded air core induction coil. Lack of an iron core implies significant weight savings. We further optimize the coil design, namely the coil length to outer diameter ratio and the outer diameter to inner diameter ratio, so as to maximize the output voltage with respect to noise in the intended axial direction. Digital signal processing (DSP) is finally applied to reduce the noise level. Key to our DSP method is a bandpass filter that rejects signals outside the intended MCG frequency range followed by a cycle averaging approach. As a proof-of-concept, *in vitro* measurements demonstrate the feasibility of our induction coil sensing system to capture MCG signals using 4 coil sensors and only 15 minutes of recording time. Expectedly, results are readily scalable to coil arrays of diverse numbers of coil sensors.

Section II discusses the operating principle and design of the proposed sensing system. Section III presents the *in vitro* experimental set-up, while Section IV reports experimental results. The paper concludes in Section V.

II. Methods and Procedures

A. System Overview

The proposed sensor operates based on Faraday's law: the changing magnetic flux of the heart is captured by an array of induction coils placed against the chest, leading, in turn, to the generation of time-varying voltages across the coils' terminals. Capturing this changing voltage is a means of monitoring the magnetic field activity of the heart. Theoretically, one sensing coil would be sufficient to couple to the magnetic field of the heart. But, in practice, the low amplitude of the heart's magnetic field necessitates a multitude of sensing coils to concurrently capture the signal so that noise can be brought down via DSP within a reasonable amount of recording time (i.e., a few minutes). A tradeoff in this case is that the number of coils used to average the recorded signals limits the sensor's imaging resolution. As such, optimal array designs should include numerous coils, groups of which image MCG activity under their corresponding surface. As an example, Fig. 1 shows a coil array that fits up to 7 groups of coils (namely 'big fixture holder'). Inside each holder, a 'small coil fixture' can be inserted that includes multiple coils (up to 7 in the case of Fig. 1) for signal averaging. Notably, designs such as that of Fig. 1 are adaptable, i.e., different numbers of coils and in different configurations may be employed for MCG retrieval, per clinical situation (intended imaging resolution, time available, noise levels, and so on). Here, we report proof-of-concept results for a total of 4 coils, noting that the process is readily scalable to coil arrays of diverse sizes.

The block diagram of our coil sensing system is shown in Fig. 2. As seen, the heart's magnetic field is first picked up by the array of MCG coil sensors. Due to the signal's extremely weak magnitude (i.e. ~10^{-6} Gauss) [11], MCG coils are connected to an amplifier board that amplifies their recorded signal by 1000 times. Key to the success of our design is that the amplifiers are placed far away from

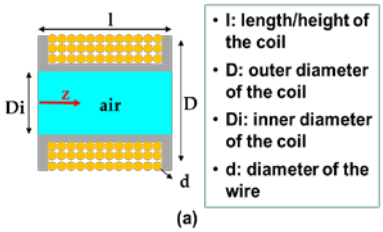

Coil Parameters	Value
l [mm]	11
D [mm]	15
Di [mm]	9.3
d [mm]	0.2
Weight [g]	8.5

Fig. 3. (a) Coil design parameters. (b) Optimized coil parameters values.

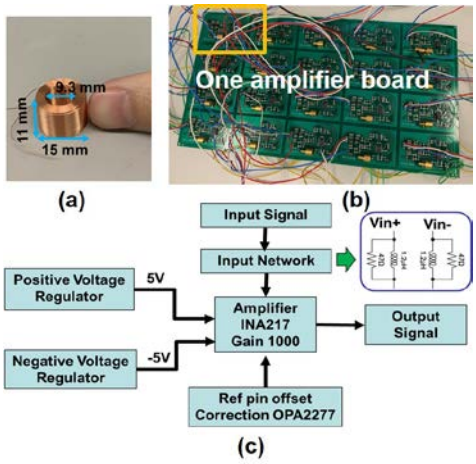

Fig. 4. (a) MCG coil sensor employed in this work. (b) 20 amplifier boards integrated into a single circuit board. (c) Amplifier circuit overview

the coils so that electric signals from the amplifier board are not captured by the sensor. The amplified signals are then picked up by a multi-channel analog to digital convertor (ADC) and sent on for further processing. The ultimate aim from this stage on is to retrieve the MCG signal from the noise floor via advanced DSP, as will be explained in Sec. II.C. Here, it is worth mentioning that key to our DSP process is the collection of a concurrent ECG signal. Since ECG is synced with MCG (via a derivative relationship), ECG serves to identify the MCG cycles which are otherwise hidden under the noise floor. A 3-lead ECG sensor is indicated in Fig. 2, but a pulse (or other) sensor may be alternatively used.

B. MCG Coil Sensor Design

The proposed induction coil sensor is designed based on the model of a tightly winded air core coil. To our knowledge, this is the first time that air-cored coils are reported for MCG detection, serving to reduce the overall weight by over 216 times as compared to previous works [25]. Fig. 3(a) shows the side view of our coil design. Parameters subject to optimization include: (a) the coil's length/height, l, (b) its outer diameter, D, (c) its inner diameter, D_i, and (d) the diameter of the wire used, d.

Our goal is to design the coil sensor for maximum sensitivity (S) along the z direction (per the coordinate system of Fig. 3(a)) when given a fixed magnetic flux density (B) at a fixed frequency (f). Here, high sensitivity implies large output voltage with respect to noise. The output voltage of an induction coil (V) can be calculated as [26]:

$$V = An\frac{\Delta B}{\Delta t} = 2\pi^2 fnR_a{}^2 B \tag{1}$$

where R_a is the average radius of the coil, A is the surface area of the coil, and n is the number of coil turns. Considering the coil to be tightly winded, Eq. (1) can be rewritten using the four optimization parameters as:

$$V = \frac{\pi^2 flB}{16d^2}(D - Di)(D + Di)^2 \tag{2}$$

The noise, namely thermal Johnson noise (V_T), produced by our coil can be expressed as:

$$V_T = 2\sqrt{k_B T\Delta f R} = \frac{2\sqrt{k_B T\Delta f l\rho(D+Di)(D-Di)}}{d^2} \tag{3}$$

where R is the coil resistance, k_B is the Boltzmann constant, T is the coil's absolute temperature in Kevin, d is the diameter of the wire, and ρ is the wire resistivity. For maximum sensitivity along the z direction (per Fig. 3(a)), the coil parameters need to follow [27]:

$$\frac{l}{D} = \frac{3}{\sqrt{20}}\sqrt{\frac{1-\left(\frac{Di}{D}\right)^5}{1-\left(\frac{Di}{D}\right)^3}} \tag{4}$$

Using Eq. (2), (3) and (4), the sensitivity can be expressed as:

$$S = \frac{V}{BV_T} = \frac{\sqrt{3}\pi^2 f(D+Di)\sqrt{D}}{32\cdot 20^{\frac{1}{4}}\sqrt{k_B\Delta f\rho T}}\cdot\left[\frac{1-\left(\frac{Di}{D}\right)^5}{1-\left(\frac{Di}{D}\right)^3}\right]^{\frac{1}{4}}\sqrt{(D^2-Di^2)} \tag{5}$$

Here, it is worth noting that d does not play any role in determining the coil sensitivity (S). Given fixed values for the coil length/height (l), outer diameter (D) and inner diameter (Di), an increase in the wire diameter will decrease the signal level. In the meantime, with fixed l, D and Di, an increase in wire diameter will also decrease the thermal Johnson noise. When calculating the sensitivity, these two effects will eventually cancel out the impact of d.

Assuming a fixed frequency and temperature, Eq. (5) can be rewritten as:

$$\frac{S}{D^{2.5}} = M\left(1+\frac{Di}{D}\right)\left[\frac{1-\left(\frac{Di}{D}\right)^5}{1-\left(\frac{Di}{D}\right)^3}\right]^{\frac{1}{4}}\sqrt{\left(1-\left(\frac{Di}{D}\right)^2\right)} \tag{6}$$

where *M* is a positive real value. Eventually, Eq. (6) can be used to identify the optimal coil design with the highest sensitivity given fixed values for B and f. It is found that when Di/D ≈ 0.6 and l/D ≈ 0.7, the coil's sensitivity is maximized. Concurrently, larger values of D while maintaining the same Di/D and l/D ratios will achieve higher sensitivity as compared to smaller values of D. This is because when the two ratios are kept the same, S is proportional to $D^{2.5}$, meaning that larger values of D will result in higher sensitivity. In our case, given that coil miniaturization is of paramount importance, we select D=15mm, and fine-tune the rest of the coil design parameters so as to fit the ratios above. The final coil parameters are given in Fig. 3(b) with the coil prototype shown in Fig. 4(a). Notably, this coil sensor is: (a) 4.67 times smaller in diameter and 4.5 times smaller in height than [25],

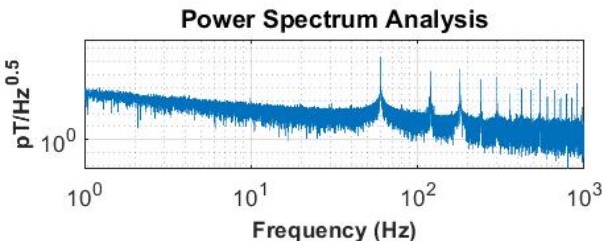

Fig. 5. Sensitivity of the proposed system (coil sensor and the amplifier) measured in a non-shielded environment.

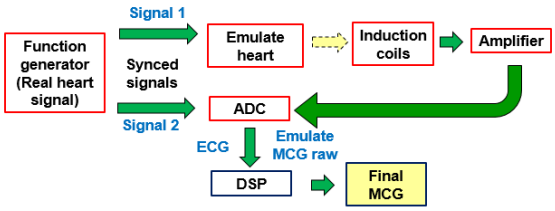

Fig. 6. Block diagram showing an overview of our experimental set-up.

and (b) at least 216 times lighter than [25].

The amplifiers used to amplify the raw coil signals by 1000 times (per Fig. 2 and Section II.A) are shown in Fig. 4(b). The circuit overview is shown in Fig. 4(c). Improving upon [25], our new amplifier design adds an input network that eliminates oscillations at the input port. The input network consists of two inductor/resistor pairs connected to the positive and negative ports of the input signal and is further connected to an amplifier (INA217). We note that our coil sensor has very low impedance (~3.5 Ω) which is desirable for the chosen amplifier that has a very low voltage noise and a relatively high current noise [28]. Given the low source impedance, the current noise will not contribute much to the application. On the other hand, a very low source impedance (<10Ω) might cause the instrumental amplifier to oscillate [28]; our input network greatly reduces any oscillation tendencies [28]. As another improvement, our design places the amplifiers far away from the sensor coils so as to eliminate noise per Section II.A. By contrast, the design in [25] placed each amplifier right atop of each coil, hence degrading sensitivity. To further eliminate vibration noise across multiple amplifiers, all amplifiers are integrated into a single board (20 amplifiers shown in the example prototype of Fig. 4(b)).

To demonstrate the sensitivity, the noise floor of the proposed system (coil sensor and the amplifier) is measured inside a non-shielded environment – as the targeted operation environment for our sensor. The power spectrum density in this case is shown in Fig. 5. A uniform magnetic field provided by a Helmholtz coil is used to convert the voltages to magnetic field strength. At 10 Hz, the noise level is measured to be 70 pT/√Hz, while at 100 Hz, the noise level is measured to be 5.08 pT/√Hz.

C. Digital Signal Processing

As expected, signals captured by the ADC need extensive DSP before they can be de-noised and depict a clear MCG signal. Our proposed DSP process involves 6 steps and is hereafter described considering *m* number(s) of coils used to capture the cardiac signal from one target area. Of course, the proposed system and accompanying DSP process have the ability to scale up and detect MCG signals across any number of target areas:

Step 1. Raw signal collection: Both MCG and ECG signals are collected simultaneously for a period of time. In turn, the ADC collects *m* sets of "raw MCG" signals (namely, raw_MCG$_1$, raw_MCG$_2$ … raw_MCG$_m$) and one set of ECG signal. We note that capturing raw signals over a period of time is critical so that uncorrelated noise can be cancelled out at a later stage.

Step 2. Bandpass filtering: For each set of collected "raw MCG" signals, bandpass filtering is employed to eliminate noise outside the intended MCG frequency range (i.e. 8-35 Hz) [29]-[32]. This process generates *m* sets of "filtered MCG" signals (namely, filtered_MCG$_1$, filtered_MCG$_2$ … filtered_MCG$_m$).

Step 3. Cutting to viewing windows: The collected ECG signal is synced with each set of "filtered MCG" signals. Using the ECG R-peak as a guide, each set of "filtered MCG" signals is cut into *N* viewing windows, with the synced ECG R-peak located in the middle of each viewing window. The duration of each viewing window (1 sec in our case) is selected such that each viewing window contains information on one cardiac cycle. For example, filtered_MCG$_1$ is cut into MCG$_1$_viewing_wdw1, MCG$_1$_viewing_wdw2 … MCG$_1$_viewing_wdw*N* .

Step 4. Averaging viewing windows: All viewing windows are averaged for each set of "filtered MCG", generating *m* sets of averaged MCG, namely MCG$_1$_ave, MCG$_2$_ave… MCG$_m$_ave. In doing so, uncorrelated noise is eliminated. Within each set of averaged MCG, all *N* viewing windows are added up and divided by *N*.

Step 5. Multiple sensor averaging: The *m* sets of averaged MCG signals resulting from *Step 4* (i.e., MCG$_1$_ave, MCG$_2$_ave… MCG$_m$_ave) are then averaged to generate a single averaged MCG signal (i.e., MCG_ave).

Step 6. Final signal: Depending on the coil array configuration, the final MCG signal can be a combination of diverse values of MCG_ave. For example, a set of coils can be placed on the top left side of the heart capturing an averaged positive magnetic field (MCG_ave_positive), while another set of coils can be placed on the opposite side of the heart to pick up the averaged negative magnetic field (MCG_ave_negative). In this case, the two MCGs can be independently visualized, or they can be subtracted from each other to result in a single MCG value (i.e., final_MCG = MCG_ave_positive - MCG_ave_negative). The latter will be the case followed in our *in vitro* experimental setup.

III. EXPERIMENT

To validate our proposed coil array, we aim to: a) identify the minimal signal level that the system can detect in a non-shielded environment, and b) compare this signal level vs. the actual signal level generated by the human heart. An

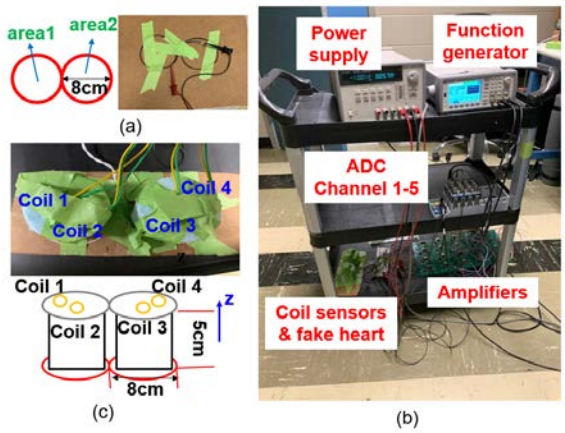

Fig. 7. (a) 8-shaped emulate heart. (b) Overview of the experimental set-up. (c) Overview of the 4 sensing coils placed upon the emulate heart.

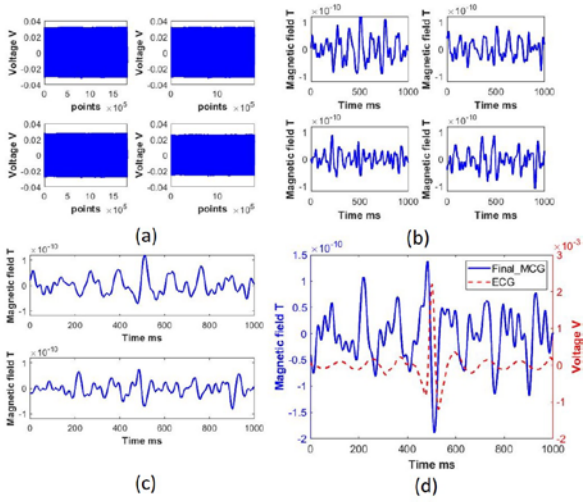

Fig. 8. (a) Raw signal data from each individual coil. First row (left to right): area1_raw_MCG$_1$, area1_raw_MCG$_2$, and second row (left to right): area2_raw_MCG$_1$ and area2_raw_MCG$_2$. (b) Processed data after *Step 4* of the DSP process. First row (left to right): area1_MCG$_1$_ave, area1_MCG$_2$_ave, and second row (left to right): area2_MCG$_1$_ave, area2_MCG$_2$_ave. (c) Averaged signal from each area obtained after *Step 5*. First row: area1_MCG_ave, and second row: area2_MCG_ave. (d) The final averaged signal (final_MCG) obtained through *Step 6*.

overview of our *in vitro* experimental set-up is shown in Fig. 6. Here, the function generator is outputting two identical ECG signals (as originally recorded by the human heart) indicated as "signal 1" and "signal 2", respectively. "Signal 2" heads directly to the ADC and is used as an ECG that will be used later in the process to identify each cardiac cycle during the DSP process. By contrast, "signal 1" heads towards an emulate heart (see Fig. 7(a)), i.e., an 8-shaped coil that serves to generate the corresponding magnetic signal, namely the emulate MCG. The latter is picked up wirelessly though our coil array. Eventually, the collected emulate MCG and ECG are both converted to digital signals via a multi-channel ADC. A Helmholtz coil is used to calibrate the system by providing a uniform magnetic field surrounding our coil sensor. Specifically, our coil sensor is placed in the middle of the Helmholtz coil with known uniform magnetic field passing through it. This known field is used to calibrate the unit from Voltage to Tesla. Then, though DSP, the "final MCG" signal is retrieved. Here, it is worth noting that the 8-shaped emulate heart employs the two circles winded in the opposite direction, each with a diameter of 8cm. When feeding the emulate heart with an electric signal, the opposite-directed windings create a magnetic field that comes out of one loop (area 1 in Fig. 7(a)) and then heads into the second loop (area 2 in Fig. 7(a)). This magnetic field map closely resembles the real MCG signal over the human chest shown in [33].

As a proof-of-concept, we employ 4 coil sensors to detect MCG signals upon two areas of the emulate heart (2 coil sensors per area), as shown in Fig. 7(b). All 4 sensors are placed 5 cm away from the "heart" to emulate a typical torso size, with foam being used to elevate the sensors. The overall experimental set-up is shown in Fig. 7(c). A 24-bit multi-channel ADC by National Instruments is used, powered at ±10V and set to sample at 2,000 Hz across its 5 channels (4 channels for the coil sensors and 1 channel for the ECG). The amplifier board is purposely placed away from the sensing array so as to eliminate the risk of the amplifier electric signal being picked up by the coils. Labview® is used to interface with the ADC. Our experiment ran for 30 minutes, yet only 15 minutes were sufficient to produce a clear final_MCG signal, per Section II.C.

IV. Results

A. Detection Sensitivity

With the function generator outputting a 2mV peak-to-peak (pk-pk) ECG signal, and by using the 4 coil sensor array with only 15 minutes of recording time, the final_MCG signal can be retrieved, Fig. 8. More specifically, Fig. 8(a) shows the obtained raw MCG signals (namely area1_raw_MCG$_1$, area1_raw_MCG$_2$, area2_raw_MCG$_1$, area2_raw_MCG$_2$). As expected, these raw signals are very noisy and MCG activity is buried under the noise floor. Data from areas 1 and 2 are then processed separately, following the process of Section II.C. That is, *Steps 1* to *4* transform the raw signals to the averaged ones (namely, area1_MCG$_1$_ave, area1_MCG$_2$_ave, area2_MCG$_1$_ave, area2_MCG$_2$_ave), as shown in Fig. 8(b). Note here that, since not all coils are placed in the exact location with respect to the emulate heart (see Fig. 7(c)), the magnetic signals that are being picked up by each of the 4 coil sensors are different. Then, *Step 5* generates the area1_MCG_ave and area2_MCG_ave, as shown in Fig. 8(c). Based on the coil array configuration, the final averaged MCG signal can be obtained via subtraction (final_MCG = area1_MCG_ave - area2_MCG_ave). This is reported as *Step 6*, shown in Fig. 8(d), where the blue line represents the final_MCG signal and the red line represents the corresponding averaged ECG signal. As seen, the processed MCG signal has a clear peak that is also synced with the corresponding ECG R-peak. This proves that the collected MCG signal is indeed a real one. Note that averaging the data for a period of time so as to obtain the final MCG is common practice for most of the existing MCG sensors, including SQUID-based sensors and other

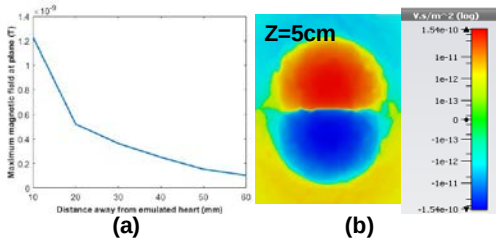

Fig. 9. (a) Maximum Z-component of the magnetic field B at planes with different distance away from the emulated heart. (b) Z-component of B generated by the emulated heart at the plane where the recording coils are placed (z = 5 cm).

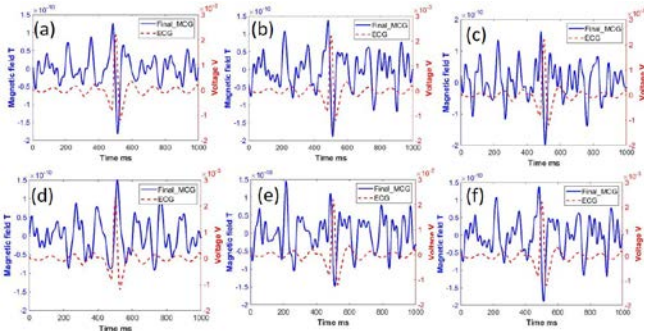

Fig. 10. Processed final averaged signal (final_MCG) of all 4 coil sensors using (a) 30 min, (b) 15 min, and (c) 6 min of recording time. Processed final averaged MCG signal using 15 minutes recording time when (d) 1 coil sensor is used to detect 1 area, (e) 2 coil sensors are used to detect 2 areas, and (f) 4 coil sensors are used to detect 2 areas.

commercial devices [25] [34]-[37]. A number of cardiac conditions, such as coronary artery disease (CAD), can be identified by the averaged MCG signal [38].

Transitioning from the aforementioned *in vitro* set-up to a real-world *in vivo* set-up, we note that the human heart MCG is ~10^{-6} Gauss [11]. Considering the set-up of Fig. 7, when inputting a 2 mV pk-pk signal into the emulated heart, the induced current is calculated to be 40 μA pk-pk. With these in mind, our experimental setup was simulated in CST's low frequency solver to confirm its capability of detecting magnetic signals in the ~10^{-6} Gauss range. In simulations, a 50 Hz sinusoidal current of 40 μA pk-pk was used as the excitation signal fed into the 8-shaped coil. We note that the 50 Hz frequency is selected as an example scenario that lies within the range of our frequencies of interest. As would be expected, the maximum absolute magnetic field occurs at each ¼ (0.005s, 0.025s …) and ¾ (0.015s, 0.035s …) wave cycle. For these time instants, Fig. 9(a) shows that the maximum z-component magnetic field is increasingly stronger as the viewing plane gets closer to the emulated heart. Fig. 9(b) shows the z-component of the magnetic field at the z = 5 cm plane (typical chest size) where our sensing coils are placed (z direction shown in Fig. 7(c)). As seen, the maximum absolute z-direction field strength at the plane where the detection coil sensors are placed is 1.54 ×10^{-6} Gauss. This value lies in the range of a typical human heart MCG. That is, we can safely assume that our MCG sensing system has the ability to detect human heart signals with 15 min of recording time. We note that this performance is not achieved by the coils themselves, but rather by a combination of the coils and the associated DSP algorithms. Without DSP, MCG signals cannot be retrieved from the raw data captured by the coils (i.e., they are buried under the noise floor). Higher levels of MCG signals can easily be detected using the same system with less recording time and/or less recording coils (i.e., less averaging windows). The key to actually picking up the MCG signals from an unshielded environment is the DSP. In vivo validation is outside the scope of this work, but will be performed in the future.

B. *Parametric Studies*

Several experimental studies have been carried out to assess the effect of varying recording time and varying number of recording coils. For example, Fig. 10 compares the final_MCG signal acquired using the 4-coil array of Fig. 7 with 30 min (Fig. 10 (a)), 15 min (Fig. 10 (b)) and 6 min (Fig. 10 (c)) of recording time. As seen, longer recording times produce a much clearer signal. This is because with decreasing recording time, a smaller number of viewing windows is averaged. In turn, less uncorrelated noised is canceled out and the processed final signal will have higher noise levels. Similarly, when the signals are averaged over an increased number of recording coils, the final_MCG is anticipated to be much clearer. Indeed, considering 15 min of recording time, Fig. 10 compares the final_MCG when using 1 (Fig. 10 (a)), 2 (Fig. 10 (b)) and 4 (Fig. 10 (c)) coils.

Depending on the clinical situation and application scenario (intended imaging resolution, time available, noise levels, and so on), different recording times and number of recording coils can be eventually selected.

V. Conclusion

In this paper, we presented a lightweight and miniaturized passive induction coil sensing system that has the ability to monitor human MCG activity in non-shielded environments. The proposed array consists of coils, each having an outer diameter of 15 mm and a height of 11 mm, and weighing less than 8.5 g. Compared to previous works in the field, our sensor is (a) 4.67 times smaller in diameter and 4.5 times smaller in height, and (b) at least 216 times lighter.

Notably, *in vitro* experimental results indicated that our proposed system has the ability to detect 2mV pk-pk source signal strength within only 15 min of recording time. This level was deemed adequate to retrieve human MCG under *in vivo* scenarios. Though outside the scope of our current work, *in vivo* studies will be performed in the future. Leveraging our proposed 3D-printed coil fixtures, arrays of diverse number of coils and pattern configurations can be eventually employed to fit different clinical needs. For example, a higher number of coils, much like a longer recording time, were shown to improve the signal clarity.

Overall, our proposed coil sensor array brings forward unprecedented opportunities for the future of cardiac activity sensing in a non-invasive and more comfortable manner for the patients.

REFERENCES

[1] R. Sameni and G.D. Clifford, "A Review of Fetal ECG Signal Processing; Issues and Promising Directions," *Open Pacing Electrophysiol Ther J*, 2010.

[2] E.A.P. Alday, C. Zhang, M. A. Colman, H. Ni, Z. Gan and A.H. Zhang, "Comparison of electric- and magnetic- cardiograms produced by myocardial ischemia in models of the human ventricle and torso," in *Computing in Cardiology Conference(CinC)*, 2015.

[3] S. Yamada and I. Yamaguchi, "Magnetocardiograms in Clinical Medicine: Unique Information on Cardiac Ischemia, Arrhythmias, and Fetal Diagnosis," *Internal Medicine*, vol. 44, no. 1, pp. 1–19, 2005.

[4] F.E. Smith, P. Langley, P.V. Leeuwen, B. Hailer, L. Trahms, U. Steinhoff, J.P. Bourke and A.A. Murray, "Comparison of magnetocardiography and electrocardiography: a study of automatic measurement of dispersion of ventricular repolarization," *EP Europace*, vol. 8, p. 887–893, 2006.

[5] M. Linzer, E H. Yang, M. Estes III, P. Wang, V.R. Vorperian and W.N. Kapoor, "CLINICAL GUIDELINE: Diagnosing Syncope: Part 1: Value of History, Physical Examination, and Electrocardiography," *Annals of Internal Medicine*, pp. 989-996, 1997.

[6] V. Mäntynen, T. Konttila and M. Stenroos, "Investigations of sensitivity and resolution of ECG and MCG in a realistically shaped thorax model," *Physics in Medicine & Biology*, p. 7141–7158, 2014.

[7] G. Pei, J. Wu, D. Chen, G. Guo, S. Liu, M. Hong, and T. Yan, "Effects of an Integrated Neurofeedback System with Dry Electrodes: EEG Acquisition and Cognition Assessment," *Sensors*, vol. 18, no. 10, p. 3396, Nov. 2018.

[8] Y. Wang and L. Guo, "Nanomaterial-Enabled Neural Stimulation," *Frontiers in Neuroscience*, vol. 10, Jul. 2016.

[9] R.F. Riley, L.K. Newby, C.W. Don, M.T. Roe, D.N. Holmes, S.K. Gandhi, M.A. Kutcher and D.M. Herrington, "Diagnostic Time Course, Treatment, and In-Hospital Outcomes for STEMI Patients Presenting with Non-Diagnostic Initial ECG: A Report from the AHA Mission: Lifeline Program," *American Heart Journal*, vol. 165, no. 1, pp. 50-56, 2013.

[10] R. Fenici, D. Brisinda, and A.M. Meloni, "Clinical application of magnetocardiography," *Expert Review of Molecular Diagnostics*, vol. 5, no. 3, pp. 291–313, 2005.

[11] D. Cohen, "Magnetoencephalography: Evidence of Magnetic Fields Produced by Alpha-Rhythm Currents," *Science* , vol. 161, no. 3843, pp. 784-786, 1968.

[12] G. M. Baule and R. McFee, "The magnetic heart vector," *American Heart Journal*, vol. 79, no. 2, pp. 223-236, 1970

[13] K. Kobayashi, Y. Uchikawa, K. Nakai and M. Yoshizawa, "Analysis and estimation of excitation conduction with Wolff-Parkinson-White syndrome patients based on a 3-D magnetocardiogram," *IEEE Transactions on Magnetics*, vol. 38, no. 5, pp. 3338-3340, 2002.

[14] Elekta, "Elekta technology virtually eliminates MEG helium refills," *Elekta AB*. [Online]. Available: https://www.elekta.com/meta/press-intern/?id=c9c8fa2c-349a-4835-bd8b-78231ec2729c. [Accessed: 29-Jan-2020].

[15] M. I. Faley, J. Dammers, Y. V. Maslennikov, J. F. Schneiderman, D. Winkler, V. P. Koshelets, N. J. Shah, and R. E. Dunin-Borkowski, "High-TcSQUID biomagnetometers," *Superconductor Science and Technology*, vol. 30, no. 8, p. 083001, 2017.

[16] H. T. Brake, A. Rijpma, J. Stinstra, J. Borgmann, H. Holland, H. Krooshoop, M. Peters, J. Flokstra, H. Quartero, and H. Rogalla, "Fetal magnetocardiography: clinical relevance and feasibility," *Physica C: Superconductivity*, vol. 368, no. 1-4, pp. 10–17, 2002.

[17] T. H. Sander, J. Preusser, R. Mhaskar, J. Kitching, L. Trahms, and S. Knappe, "Magnetoencephalography with a chip-scale atomic magnetometer," *Biomedical Optics Express*, vol. 3, no. 5, p. 981, 2012.

[18] D. Sheng, S. Li, N. Dural, and M. V. Romalis, "Subfemtotesla Scalar Atomic Magnetometry Using Multipass Cells," *Physical Review Letters*, vol. 110, no. 16, 2013.

[19] J. Iivanainen, M. Stenroos, and L. Parkkonen, "Measuring MEG closer to the brain: Performance of on-scalp sensor arrays," *NeuroImage*, vol. 147, pp. 542–553, 2017.

[20] O. Alem, A. M. Benison, D. S. Barth, J. Kitching, and S. Knappe, "Magnetoencephalography of Epilepsy with a Microfabricated Atomic Magnetrode," *Journal of Neuroscience*, vol. 34, no. 43, pp. 14324–14327, 2014.

[21] V.K. Shah and R.T. Wakai, "A Compact, High Performance Atomic Magnetometer for Biomedical Applications," *Physics in Medicine & Biology*, vol. 58, 2013.

[22] T. Uchiyama and T. Takiya, "Development of precise off-diagonal magnetoimpedance gradiometer for magnetocardiography," *AIP Advances*, vol. 7, no. 5, p. 056644, 2017.

[23] D. Karnaushenko, D. D. Karnaushenko, D. Makarov, S. Baunack, R. Schäfer, and O. G. Schmidt, "Self-Assembled On-Chip-Integrated Giant Magneto-Impedance Sensorics," *Advanced Materials*, vol. 27, no. 42, pp. 6582–6589, 2015.

[24] T. Takiya and T. Uchiyama, "Development of Active Shielding-Type MI Gradiometer and Application for Magnetocardiography," *IEEE Transactions on Magnetics*, vol. 53, no. 11, pp. 1–4, 2017.

[25] J. Mooney, S. Ghasemi-Roudsari, E. Banham, C. Symonds and N.P. a. B. Varcoe, "A portable diagnostic device for cardiac magnetic field mapping," *Biomed. Phys. Eng*, vol. 3, no. 1, 2017.

[26] S. C. Mukhopadhyay, K P. Jayasundera and A. Fuchs, Advancement in Sensing Technology, Springer, 2013.

[27] H. Zijlstra, Experimental methods in magnetism, North-Holland Publ, 1967.

[28] Texas Instruments, "INA217 Low-Noise, Low-Distortion Instrumentation Amplifier Replacement for SSM2017," SBOS247C datasheet, Jun. 2002 [Revised Nov.2015].

[29] L. Tereshchenko and M. Josephson, "Frequency Content and Characteristics of Ventricular Conduction," *Journal of Electrocardiology*, vol. 48, no. 6, pp. 933-937, 2015.

[30] C.-H. Lin, "Frequency-domain features for ECG beat discrimination using grey relational analysis-based classifier," *Computers & Mathematics with Applications*, vol. 55, no. 4, pp. 680-690, 2008

[31] K. Yoshida, K. Ogata, T. Inaba, Y. Nakazawa, Y. Ito, I. Yamaguchi, A. Kandori, and K. Aonuma, "Ability of magnetocardiography to detect regional dominant frequencies of atrial fibrillation," *Journal of Arrhythmia*, vol. 31, no. 6, pp. 345–351, 2015.

[32] X. Liu, L. Pei, S. Zhang, Y. Wang, and Y. Dai, "Characteristics of magnetocardiography and electrocardiography in the time-frequency domain," *Chinese Science Bulletin*, vol. 56, no. 8, pp. 819–825, 2011.

[33] N.A. Trayanova, "Modeling of Ventricular Arrhythmias," *Cardiac Mapping*, pp. 140–149, 2012.

[34] J. Reermann, E. Elzenheimer, and G. Schmidt, "Real-Time Biomagnetic Signal Processing for Uncooled Magnetometers in Cardiology," *IEEE Sensors Journal*, vol. 19, no. 11, pp. 4237–4249, 2019.

[35] G. Rosu, M. C. Rau, and O. Baltag, "Comparison of signal processing methods applied on a magnetocardiographic signal," *2017 10th International Symposium on Advanced Topics in Electrical Engineering (ATEE)*, 2017.

[36] S. Senthilnathan, R. J. Selvaraj, R. Patel, S. Satheesh, G. Katholil, M. P. Janawadkar, and T. S. Radhakrishnan, "Noninvasive Determination of HV Interval Using Magnetocardiography," *Pacing and Clinical Electrophysiology*, vol. 40, no. 5, pp. 568–577, 2017.

[37] S. Zhang, G. Zhang, Y. Wang, J. Zeng, Y. Qiu, M. Liu, X. Kong, and X. Xie, "A novel superconducting quantum interference device for biomagnetic measurements," *Chinese Science Bulletin*, vol. 58, no. 24, pp. 2917–2919, 2013.

[38] Y. Li, Z. Che, W. Quan, R. Yuan, Y. Shen, Z. Liu, W. Wang, H. Jin, and G. Liu, "Diagnostic outcomes of magnetocardiography in patients with coronary artery disease," *Int J Clin Exp Med*, vol. 8, no. 2, pp. 2441–2446, Feb. 2015.

Keren Zhu (S'19) received the B.S. degree in electronical and computer engineering from The Ohio State University, Columbus, OH, USA, in 2017 and is currently working toward the Ph.D. degree in electrical and computer engineering at The Ohio State University.

She is currently a graduate research assistant at the ElectroScience Laboratory, Columbus, OH, USA. From May 2016 to July 2016, she was a student intern at Hangzhou TuoXing Electronic Tech Co., Hangzhou, China. Her main research interests include electromagnetics, antennas, and bio-medical sensors.

Ms. Zhu received the pre-graduate scholarship at the IEEE Microwave Theory and Techniques Society in 2018. She received Distinguished

Graduate Student Award from The Ohio State University Women in Engineering in 2018.

Adhvait M. Shah received B.S. in Biomedical Engineering from Tufts University in Medford, MA in 2012 and a PhD degree in Medical Engineering and Medical Physics from Massachusetts Institute of Technology, Cambridge, MA in 2019. His doctoral work focused on developing and evaluating biomaterials-based treatment for spinal cord injured patients.

Currently, he is contributing as a Project Engineer in Biomedical branch of Triton Systems Inc. working towards developing medical solutions for warfighters. Specifically, he is the Project Lead for the endeavor to develop non-invasive electromagnetic based solutions to diagnose and treat spinal injuries. He has also worked as an Engineering Intern at Organogenesis Inc, Canton, MA in 2011 and as Research Assistant at Orthopedic Biomechanics Laboratory at Beth Israel Deaconess Medical Center, Boston, MA in 2010. Further, he has served in various roles including as an Instructor for the Office of Minority Education, MIT, Cambridge, MA from 2012-2018.

.Dr. Shah has received Neuroimaging Training fellowship from National Institute of Biological Imaging and Bioengineering (NIBIB) from NIH for 2015-2017 period and Health, Science, and Technology fellowship from MIT during 2012-13. Dr. Shah has presented his work at several conference and has won Best Poster Award at the New England Science Symposium, Boston, MA in 2018.

Jan Berkow is the Director of Triton System's Physiologic Monitoring and Medical Device business areas. Before joining Triton, he provided consulting for several University programs and initiatives. This included crafting visions and developing go-to-market business plans for emerging technologies. As a consultant to the University of Pittsburgh Center for Military Medicine, he helped craft the vision for a next generation trauma care solution that incorporates closed-loop fluid and ventilatory control to support unmanned aerial vehicles (UAVs) of opportunity for prolonged field care applications.

Prior to this, Mr. Berkow served the inventor, co-founder, and Chief Technology Officer for Intelomed, Inc. for 12 years, a University of Pittsburgh spin-out company. As the inventor of a Class II photo-optic based cardiovascular monitoring device, he developed a treatment management solution for outpatient hemodialysis clinics to reduce the incidence of treatment intolerant cardiac events to improve patient outcomes and lower hospitalization costs. In this role, he was responsible for the entire product life cycle from concept through to manufacture and sale and was responsible for both the clinical and regulatory pathways. As part of this initiative, he authored or co-authored 9 patents related to the photo-optic device.

Prior to Intelomed, Mr. Berkow was an industrial consultant providing advanced planning and scheduling tools for make-to-order industries. He also successfully won and served as prime contractor (Applied Industrial Solutions, Inc) and PI for a multi-year, $3 million grant to develop an intelligent process control solution to improve yield and lower power use for aluminum production sponsored by the Department of Energy with partners Century Aluminum, the largest domestic producer of aluminum, and West Virginia University. Mr. Berkow holds an undergraduate degree in physics and an MBA.

Asimina Kiourti (S'10, M'14, SM'19) received the Diploma degree in electrical and computer engineering from the University of Patras, Patras, Greece, in 2008, the M.Sc. degree in technologies for broadband communications from University College London, London, U.K., in 2009, and the Ph.D. degree in electrical and computer engineering from the National Technical University of Athens, Athens, Greece, in 2013.

She is currently an Assistant Professor of Electrical and Computer Engineering at The Ohio State University and the ElectroScience Laboratory, Columbus, OH, USA. From 2013 to 2016 she served as a Post-Doctoral Researcher and then a Senior Research Associate at the ElectroScience Laboratory. During her career, she has authored over 50 journal papers, 80 conference papers, 9 book chapters and 8 patents. Her research interests include bio-electromagnetics, wearable and implantable antennas, sensors for body area applications, and functionalized e-textiles.

Dr. Kiourti has received several awards and scholarships, including the URSI Young Scientist Award for 2018, the IEEE Engineering in Medicine and Biology Society (EMB-S) Young Investigator Award for 2014, the IEEE Microwave Theory and Techniques Society (MTT-S) Graduate Fellowship for Medical Applications for 2012, and the IEEE Antennas and Propagation Society (AP-S) Doctoral Research Award for 2011. She is currently serving as a Senior Associate Editor for the IEEE Open Journal of Antennas and Propagation, and an Associate Editor for the IEEE Transactions on Antennas and Propagation and the IEEE Journal of Electromagnetics, RF and Microwaves in Medicine and Biology.